John Allen

Advances in Audiology
Editor: M. Hoke, Munster

Reprint
Publishers: S. Karger, Basel
Printed in Switzerland

Grandori F, Hoke M, Romani GL (eds): Auditory Evoked Magnetic Fields and Electric Potentials. Adv Audiol. Basel, Karger, 1990, vol 6, pp 40–69

Fundamentals of Dipole Source Potential Analysis

Michael Scherg

Psychoacoustics and Evoked Potentials Laboratory, Department of Neuropsychology, Max Planck Institute for Psychiatry, Munich, FRG

Introduction

During the last decade, new techniques like color mapping of the potential distribution over the scalp [Duffy et al., 1979; Desmedt et al., 1987], dipole source localization methods [Kavanagh et al., 1978; Sidman et al., 1978, Grandori, 1984, 1986; Scherg and von Cramon, 1985a, b, 1986a] and magnetoencephalography [for reviews see Hari and Ilmoniemi, 1986; Hari, 1990, pp. 222–282, this volume] have prompted the search for the neural generators of evoked potentials and EEG. With these techniques, the focus of interest has shifted from an analysis of waveforms, derived at selected scalp sites, to the spatial potential distribution over the scalp, analyzed at selected times. Thereby, the problem of selecting an appropriate reference was replaced by the problem of selecting appropriate latencies, at which a hopefully simple source configuration would underly the scalp map. A priori, these instances need not correspond to major peaks in selected recording channels or to instances of maxima in global field power [Lehmann and Skrandies, 1980].

The major issue in topographic analyses is the location of the neural tissues within the brain which are the generating sources of a particular instantaneous scalp map. This is either done qualitatively by an interpretation of focal maxima and minima in the map or quantitatively by dipole localization methods [Wood, 1982]. However, the number of independent parameters underlying a single instantaneous scalp map is only less or equal to the number of recording channels. Hence, not much more than a single

equivalent dipole, which already has 6 coordinates, can be extracted with confidence [Fender, 1987]. Further, the location of this equivalent dipole does not necessarily coincide with the loci of the activated brain structures, if not a single but multiple sources underly the actual scalp map [Wood, 1982]. Due to this nonuniqueness of the inverse problem, i.e. the calculation of the exact source configuration from the empirical scalp topography, dipole analysis methods are facing some skepticism.

Considering these limitations, one may take a different standpoint and ask whether a combined spatiotemporal approach would not greatly enhance the possibilities of dipole source analyses [Scherg, 1984; Scherg and von Cramon, 1985a, b; Maier et al., 1987]. Furthermore, a precise definition of the equivalent of a model dipole, as demanded by Wood [1982], in conjunction with reasonable spatial constraints (hemispheric symmetry, etc.), can reduce the source problem such that a unique solution exists for a certain hypothesis [Scherg and von Cramon, 1985a, 1986a]. This can then be tested and compared with competitive hypotheses. For example, by using available information from anatomy and physiology, we may construct an electric model of the head, place equivalent model sources within all structures known or assumed to respond to a certain stimulus and attempt to explain the complete evoked potential data set over space and time by such a model. Then one may ask: What is the temporal course of activity in each of the structures? Is the activity reduced or delayed in one of these structures, if we analyze a patient's recording? Are there any other structures that become activated in relation to the stimulus or can the scalp potential distribution over time be fully explained by sources only within these few anatomical structures, which are most likely involved in the processing of the stimulus? And last, but not least, are our bioelectric data and the model accurate enough to answer such questions at all? The principle behind this approach is to put forward different hypotheses as to the origin of an evoked potential, to construct related models in space *and* time and to test them against a measured set of evoked potential data.

It appears necessary, not only for clinical applications but also for our understanding of the brain electric fields and scalp potentials, to adopt this more comprehensive view. Localization is only one and not the major goal. Of more importance and easier to extract, as it will turn out, is the compound activity of a circumscribed brain area and its temporal evolution. Therefore, the aim of this chapter is to outline how a set of measured scalp potential data can be reduced and transformed into relevant information about the underlying spatiotemporal source configuration. The principles we will describe

hold generally for any evoked or ongoing electric or magnetic brain activity, but emphasis shall be put on providing the basis for an understanding of the generation of cortical auditory-evoked potentials.

Evidently, it is impossible to derive from the scalp potential distribution the activity of each single neuron or perhaps even to separate the activities of different cortical layers. All we can expect from scalp potential analysis is a separation of the compound activity of some distinct brain areas. In the former microscopic sense, the inverse problem of deriving the source configuration from scalp potentials cannot be solved. However, unique solutions to the inverse problem do exist, at least in a mathematical sense, if we adopt the latter macroscopic view and adequately restrict the number of compound equivalent sources [Scherg and von Cramon, 1985a; Fender, 1987]. In the following paragraphs I shall try to illustrate the physical basis for a general source model and to give a proof for this assertion by presenting a mathematical formulation of the source problem which will also elucidate the various ways toward its solution. But, before doing this, it is useful to discuss the elements which are necessary to build a macroscopic model of the processes underlying the spatiotemporally varying scalp potential distribution.

Elements of a Source Model

The Equivalent Dipole

All excitation and inhibition processes on the neuronal level are primarily mediated by transmembrane current flow. The resulting secondary current and potential distribution everywhere within and on the surface of the head can in principle be described by the volume conduction theory, based on the Maxwell equations [Nunez, 1981; Mitzdorf, 1985; Hari and Ilmoniemi, 1986]. Because intracranial current flow is relatively slow in physical terms and because the brain is a good conductor, the quasistatic approach can be used [Plonsey and Hepper, 1967], i.e. current loops are closed. This means that there is as much current flowing out of an activated neuron as there is flowing in from the extracellular space. On the microscopic level, the distribution of these current sources and sinks is quite complicated and poses a difficult problem for the interpretation of locally recorded potential waveforms [Rall, 1969]. However, from a distant recording electrode, e.g. at the scalp, the situation looks much simpler, because the distance between the centers of mass of current sources and sinks is small compared to the

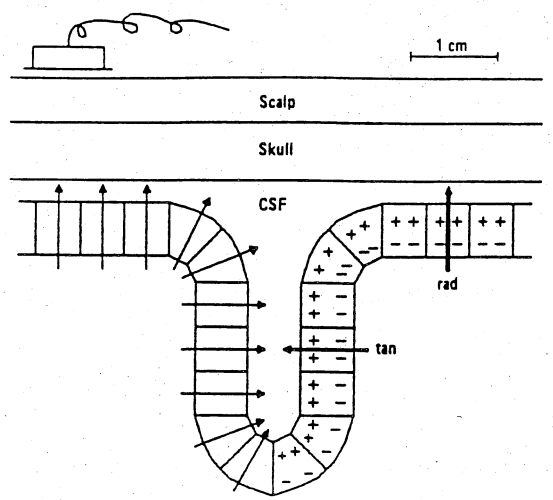

Fig. 1. Schematic diagram of a cortical fold. Due to the columnal organization of the cortex, current sources (+) and sinks (−) are displaced perpendicular to the cortical surface. This results in radial dipoles for superficial cortical segments, in tangential dipoles for fissural segments and in oblique dipoles for the banks of fissures or differently oriented fissural segments. A single radial and a single tangential equivalent dipole give a good approximation for the compound activity of all cortical segments on one side and in the vicinity of a cortical fold (right).

recording distance. Hence, the distant field can be approximated as a dipole field, whenever the effective centers of current inflow and outflow have a finite separation not exceeding a few millimeters (this would be the case only for very fast conducting peripheral nerve fibers). If the centers are very close or coincide, the distant field approaches zero.

The most important characteristic of a dipole field is its orientation. Field maxima and minima lie on opposite sides of the vector connecting the virtual centers of sinks and sources. The dipole field is zero in a plane which separates these centers and is perpendicular to the dipole vector. When a portion of cortex becomes activated, intraneuronal current flows predominantly in parallel to the vertical columns resulting in an effective vertical separation of sources and sinks and thus in a dipole field which is oriented perpendicular to the cortical surface (fig. 1). If the segment of activated cortex lies on the surface of the brain (or is parallel to the lateral convexity), the associated dipole is radial. Likewise, the activity of cortical segments lying in the depth of fissures can be approximated by tangential dipoles (fig. 1). Such

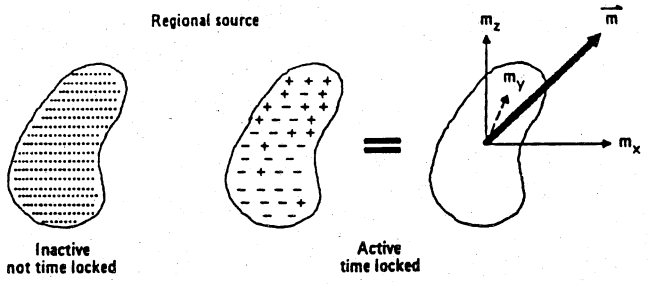

Fig. 2. Illustration of the regional source concept. The electric field due to a cerebral region containing folds or neural elements of any orientations can be approximated by a 3-dimensional dipole vector field. The dipole is located at an equivalent central location within the cerebal region and its 3 axes reflect the summed projections of the individual dipoles from each activated neural element. If the region is inactive, or does not exhibit time-locked activity, e.g. before stimulus delivery, the net distribution of current sources and sinks cancels, whereas spatially coherent displacements of sources and sinks after activation result in a net dipole field at a distant sensor.

dipoles are called equivalent because their field gives an equivalent description of the compound activity of all neuronal elements in their vicinity which are oriented in parallel to the dipole axis.

The Regional Dipole Source: Dipole Source Potentials

In principle, we may wish to subdivide the cortex into as many small planar segments as may seem necessary for an accurate description of the scalp activity (fig. 1). However, the scalp potential distribution due to nearby segments may be too similar to allow for an independent computation of the activity contributed by each segment. In this case it would be sufficient to have just a single radial and 2 tangential dipoles for a 3-dimensional model of the activity of any cortical fold within a certain brain region, no matter what orientation the various folds may have (fig. 2). This is possible, because dipoles behave like vectors, and the activity of a cortical segment at whatever inclination can be equally modeled by a single dipole perpendicular to it or by its projections onto an (orthogonal) coordinate system, which may be chosen as cartesian (x, y, z) or as a special polar coordinate system to have the convenient distinction between radial and tangential dipoles, i.e. for cortical surfaces and fissures, respectively.

Considering the time course of activation of a cortical region, we may observe a tangential dipole initially which gradually changes orientation and

ends as a radial dipole. This could be modeled by a rotating or even by a moving dipole

$$\mathbf{m} = \mathbf{m}(t); \qquad \mathbf{r} = \mathbf{r}(t); \tag{1}$$

with the dipole moment vector **m** (boldface type denotes a vector) *and* the dipole location vector **r** being functions of time. Alternatively, a good approximation for the compound activity of a limited brain region can be found by defining a 'regional dipole source' given by a dipole vector field with a stationary, time-independent location **r**, and 3 stationary dipole moment axes (e.g. 1 radial, 2 tangential in 3 dimensions). Then, the only time-varying quantities are the 3 dipole strength functions

$$\mathbf{m}(t) = [m_1(t), m_2(t), m_3(t)] \tag{2}$$

modeling the temporal variation of the dipole moment along the 3 basic axes. For a 2-dimensional montage, e.g. a coronal chain of electrodes 2 dipole axes (e.g. 1 radial and 1 tangential) are sufficient, because a dipole perpendicular to the recording plane generates an equipotential line in that plane. Using this definition of a 'regional dipole source', the locations and orientations of the 3 components of the model dipole source do not change over time, just as the underlying structures do not move over time (fig. 2). The waveforms $m_1(t)$, $m_2(t)$, $m_3(t)$ represent the time-varying magnitudes of the 3 dipole source components and are, therefore, defined as 'dipole source potentials' (apart from a scaling factor relating dipole moment to macroscopic potential units). Each dipole source potential selectively reflects activity of the underlying brain area (provided the model is correct), which is oriented in parallel with the dipole vector component. The common location for all 3 components allows the regional coordinate system to be rotated a posteriori in order to match known orientations of the underlying cortical folding, because a 3-dimensional dipole field given by this definition of a 'regional dipole source' is invariant under rotation [Scherg and von Cramon, 1986a].

The Head Model

The next element necessary for modeling scalp potentials is a head model capable of describing what the potential distribution on the scalp due to an intracranial current dipole will be. This is also called the forward problem. In principle, this relation is described in electromagnetic theory by the Poisson differential equation [Nunez, 1981; Fender, 1987], which can only be solved numerically for a realistically shaped head [Meijs et al., 1985, 1987; Hämäläinen and Sarvas, 1987]. More straightforward formulas have been shown

for models approximating the head by a sphere of homogeneous conductivity [Wilson and Bayley, 1950; Brody et al., 1973] or by several spherical shells with different homogeneous and isotropic conductivities, which electrically model the scalp, skull, cerebrospinal fluid and brain tissue [Rush and Driscoll, 1968; Kavanagh et al., 1978; Cuffin and Cohen, 1979]. The skull and scalp layers bring about an attenuation and spreading out of the potential distribution on the scalp, mainly due to the fact that the conductivity of the skull is about 80 times smaller than the similar conductivities of scalp and brain tissues.

Ary et al. [1981] have shown that the potential distribution due to a dipole at a certain depth in the more realistic 3-shell model (scalp, skull, brain) can be approximated very accurately by a somewhat deeper dipole in the homogeneous spherical head model. Scalp and skull thickness followed by the ratio of conductivity between skull and brain/scalp were the most important factors determining the attenuation and relative shift of the equivalent homogeneous sphere dipole toward the center of the sphere. The relation of dipole eccentricity, i.e. its relative distance from the center of the sphere expressed as a percentage of the head radius, in the homogeneous and 3-shell head models has been given in tabular form and graphs by Ary et al. [1981] and as an approximation function by Scherg [1984] for average head geometry and conductivities [Rush and Driscoll, 1968]. Figure 3 illustrates this approximation and the effect of the shielding layers leading to an equivalent shrinking of the electric brain to about 60% of the head diameter. Thus, surface electrodes appear to be more distant from the cranial sources and sense an attenuated and smeared-out field. This 3-shell head model approximation is very important for practical purposes, because it allows for fast computation of inverse solutions using analytic dipole formulas for the homogeneous model [e.g. Brody et al., 1973]. The resultant dipole locations are transformed to coordinates in the 3-shell head model which are already a good approximation to real head coordinates. Since only relative values of dipole moment are needed for the computation of dipole source potentials, a tranformation of dipole moment is not required. Further improvements of such transformations using realistically shaped head models may prove very useful in the future.

Any head model essentially provides functional values for the potential

$$u_k = f(\mathbf{r}, \mathbf{m}, \mathbf{e}_k) \tag{3}$$

at an electrode k located at $\mathbf{e}_k = \{e_{kx}, e_{ky}, e_{kz}\}$ due to a dipole with moment $\mathbf{m}$ at location $\mathbf{r} = \{x, y, z\}$. Because the magnitude of the dipole moment and

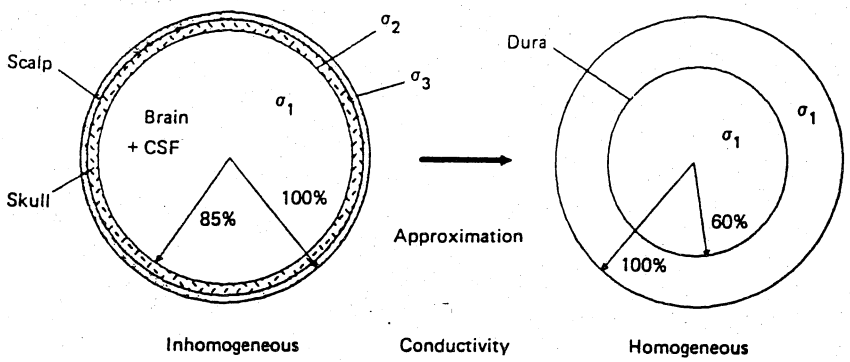

Fig. 3. Approximation of the 3-shell spherical head model by a spherical model of homogeneous conductivity. The shielding effect due to the scalp and skull (poor conductivity) layers is electrically equivalent to an effective shrinking of the brain diameter in the homogeneous sphere from approximately 84 to 60% of the head model diameter. Dipoles with accordingly transformed, i.e. reduced, eccentricity in the homogeneous sphere, produce the same scalp distribution as their equivalent, more eccentric, 3-shell model dipoles [Ary et al., 1981].

the scalp potential u_k are linearly related, we can write, including time dependence

$$u_k(t) = m(t) \cdot f(\mathbf{r}, \mathbf{o}, \mathbf{e}_k), \tag{4}$$

with **o** being the orientation of a stationary unit dipole at **r** which does not move over time. This formulation states that a single stationary dipole source contributes the same waveform m(t) to all electrodes with an attenuation function f depending only on spatial parameters, i.e. electrode location, dipole coordinates and the actual head model used.

Radial and Tangential Equivalent Dipoles

The potential distribution due to a single radial dipole is simulated in figure 4 for a coronal chain of 13 electrodes around the homogeneous spherical head model. The electrodes range from the vertex in 20-degree steps to $\pm 120°$ lateral, this approximately corresponding to the position of the earlobes. The radial dipole is pointing inward as in the situation when cortical pyramidal cells are excited at their apical dendrites, i.e. the current sinks are closer to the cortical surface than the current sources. This is the

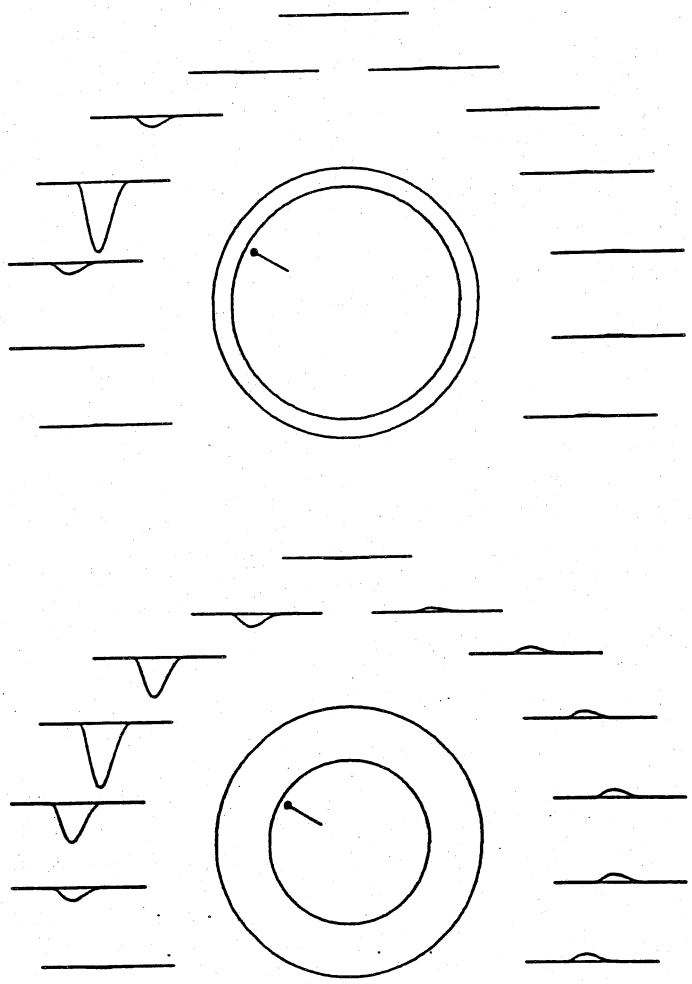

Fig. 4. Coronal scalp potential distribution of a radial equivalent dipole modeling activity of superficial cortex. The dipole is oriented inward to mimic, for example, excitatory pyramidal cell activation at the apical dendrites, producing surface negativity. neglecting the shielding effect, i.e. taking an eccentricity of about 80% in a homogeneous head model, results in a narrow focus, similar to the epicortically recorded topography (top). Adequate reduction of equivalent eccentricity results in a realistic scalp topography, which is much more widespread and exhibits a positive maximum on the opposite side of the sphere (bottom). The simulated waveforms at the vertex (C_z) and at equidistant (20°) electrodes over both hemispheres depict a monophasic activity arising with some delay after stimulus delivery.

opposite situation, as schematically illustrated in figure 1. The equivalent radial dipole is physically situated at an eccentricity of about 84% and represents activity of the superficial cortical layers in its vicinity. If we had the same homogeneous conductivity everywhere throughout the head the potential would spread only to the nearest few electrodes (fig. 4, upper half) as in epicortical records. However, due to the shielding effects of the scalp and skull layers, the real potential distribution is considerably more widespread and resembles that of a radial dipole located at an eccentricity of only about 60% in a homogeneous spherical head (fig. 4, lower half). The maximum of the negativity is focused exactly over the location of the source, but a smaller positive maximum is found on the opposite side of the sphere. Note that in real recordings, e.g. using the right earlobe as a reference, this positivity would be subtracted from each waveform.

In figure 5 the same situation is depicted for an equivalent tangential dipole reflecting the activity of fissural cortex. The scalp distribution is much more extended than in the case of the radial dipole, even when assuming a head of completely homogeneous conductivity (fig. 5, upper half). Again the real situation reflects that of a dipole at an equivalent deeper location (eccentricity 57 instead of 80%) within the homogeneous model (fig. 5, lower half). Right over the source there is no contribution from the underlying tangential dipole, whereas to both sides peaks of opposite polarity are seen. The maximum and minimum are at approximately $\pm 25°$ from the dipole source in this example. They quickly spread out further if the dipole is located deeper within the cortical fissure.

The waveforms shown in figures 4 and 5 simulate a simple physiological situation. At the beginning of each trace, e.g. at the time of stimulus delivery, no synchronous activity is present in the cortical segments. After a certain latency the number of synchronously active cells increases, reaches a maximum and decays again, thereby generating a monophasic waveform (the sink source configuration is assumed not to reverse in this simulation). Also, the compound potential contributed by a small cortical segment, i.e. the dipole source potential, has the same waveform at all scalp electrodes, because each electrode senses the same process over time. Only the overall magnitude and sign of the scalp waveforms depend on geometric factors, i.e. electrode position, dipole location and dipole orientation as given by equation 4. Thus, the source waveform, which in general is more complex, contains the information about the compound physiological processes of the source, whereas the spatial distribution of this (everywhere identical!) waveform contains the electroanatomical information about source location. The

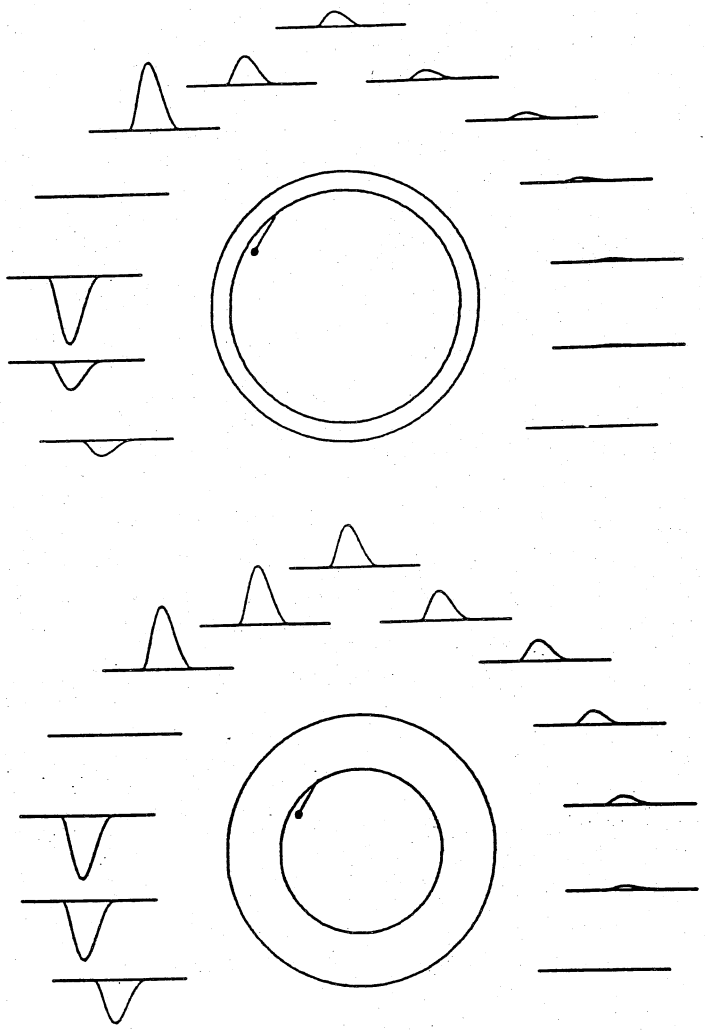

Fig. 5. Coronal scalp distribution of a tangential dipole modeling fissural cortical activity. As explained for figure 4, the correctly transformed ecentricity in the homogeneous head model (bottom) results in a realistic scalp topography with widespread positive and negative maxima to either side of the actual location of the source. Note that in the quasistatic approach a single dipole source contributes the same waveform at all electrodes. Only the attenuation factor and the sign vary with electrode site.

source problem may therefore be viewed as the problem of first extracting these dipole source potential waveforms from the scalp waveforms and then using their distribution to compute equivalent source locations.

The Superposition Principle: Spatiotemporal Overlap

Real brain sources are not ideal point sources like an equivalent dipole. One may therefore want to know how extended a brain region can be to still permit a single dipole model within a certain accuracy limit. This question and its solution by simulation is illustrated in figure 6 with realistic dipole locations. Model dipole locations were again obtained by transforming eccentricity from the 3-shell into the homogeneous model for which the simulations were computed. The size of a spherical cap of superficial cortex can be described by the solid angle it subtends as viewed from the center of the sphere. The active cortex of sensory systems does not subtend more than 20° [Vaughan, 1974]. If we subdivide this angle into smaller segments, analogous to figure 1, we may simulate the scalp potential distribution by the sum of the potentials contributed by each segmental dipole. This is legitimate because of the linear superposition principle holding for electric and magnetic fields. Then, in turn, we may adjust a single equivalent dipole to obtain a best fit (in the least-squares sense) to the simulated potential distribution, as outlined below. In order to obtain an estimate of an upper limit in inaccuracy, one may simply take the 2 dipoles which are most apart, e.g. $\pm 10°$ from the center of the cap, and compute the unexplained or residual variance (RV) in the scalp distribution for the single dipole best fit (fig. 6, top). This equivalent dipole lies only somewhat deeper (homogeneous eccentricity 60 → 53.3%) and the unexplained variance is surprisingly small (RV $< 0.21\%$) for dipole extremes at $\pm 10°$ due to the shielding effects of scalp and skull. Because of rotational symmetry is would be more accurate to simulate the effect of a 20° isoactive cap by 2 dipoles at $\pm 7.1°$. In this case, equivalent eccentricity is 56.5% and RV $< 0.05\%$ for the coronal electrode configuration depicted in figure 4 and the radial cap underlying the vertex.

Similarly, the activity of a more extended cortical fissure may be modeled by superimposing the activity of a series of segmental tangential dipoles (fig. 6, middle). Again, taking the outermost 2 dipoles for an upper bound of inaccuracy, an equivalent single dipole with 55.6% eccentricity will leave less than 0.01% of variance unexplained, if the 2 dipoles have 60 and 50% eccentricity, respectively. Single equivalent dipole eccentricity would be 52.2% and RV $< 0.05\%$ for 2 tangential dipoles located at 60 and 40% of the head radius in the homogeneous head model. Thus, the use of

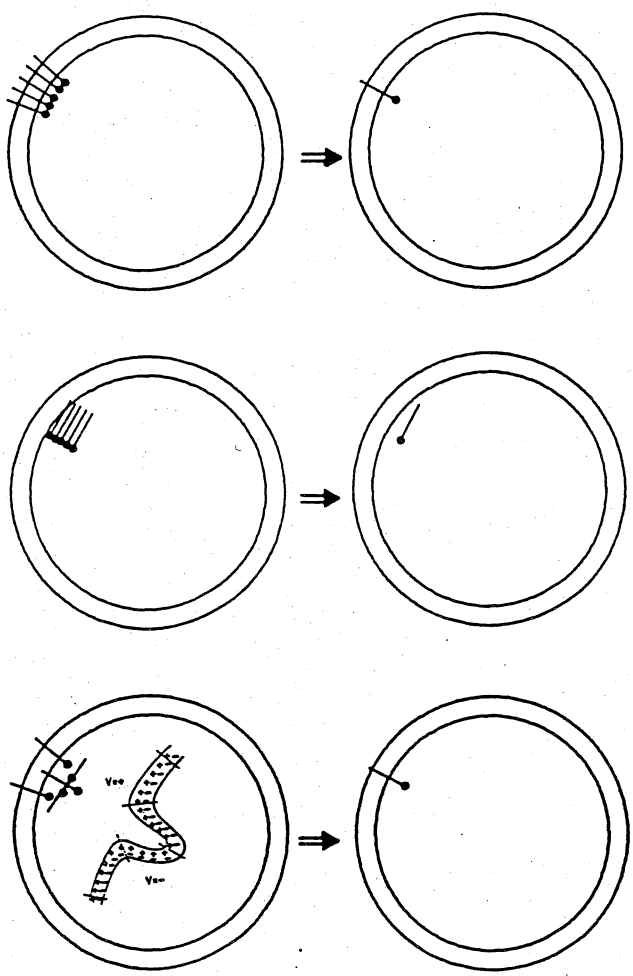

Fig. 6. Equivalent representation of activity in more extended cortical segments by single dipoles. The scalp distribution due to a cortical cap spanning a solid angle of less than 20° (top), or due to a fissural sector less than 3 cm deep (middle) is almost indistinguishable from the topography of the single equivalent dipole (see text). Synchronous activation of both sides of a cortical fold results in a radial dipole field, because the dipole fields from the opposite walls of the fissure cancel (bottom).

single radial and tangential equivalent dipole components presents an excellent approximation for the whole electric scalp activity arising from a cortical region with a maximal extension of some 2–3 cm.

Because of the superposition principle and of the vectorial properties of dipole fields, a single instantaneous equivalent dipole approximately presents the vectorial sum of all segmental dipoles in the brain region it represents. Therefore, if all the superficial and fissural layers of a cortical region are synchronously and equally activated the net equivalent dipole will be radial because the tangential dipole vectors of both sides of a fissure cancel each other (fig. 6, bottom). However, this is a rare situation because the contributions from the different segments need not be of equal strength and may change differently over time. Thus, we must expect a complex overlap of radial and tangential activity at the scalp, even if only a small circumscribed brain area is activated.

Such a spatiotemporal overlap of scalp activity due to a single point source is simulated in figure 7. Again single tangential and radial dipoles are assumed to reflect the activity of surrounding fissural (perpendicular to the frontal section) and superficial cortex, respectively. However, the temporal course of activation of both structures is assumed to differ in latency, while both dipole source potentials are monophasic in waveform and of the same polarity as in figures 4 and 5. Radial activity is assumed to start only shortly after tangential activity has already peaked. At the scalp, due to the different spatiotemporal distribution of radial and tangential activity, an apparently complex overlap leading to a whole variety of waveforms can be seen despite the simplicity of both underlying waveforms. There happens to be only a single electrode which senses activity from just one of the dipoles, i.e. the electrode exactly over the source, which records only the waveform of the radial activity. On the other hand, at the vertex electrode, only minimal radial overlap distorts the tangential dipole source wave shape. Note again that in real recordings the potential at the reference electrode would be subtracted, leading to even more complex overlap.

To summarize the results of these simulations: the concept of a regional dipole source with 3 orthogonal single dipole components (1 radial and 2 tangential in 3 dimensions, 1 tangential in 2 dimensions) can be used as a fairly good approximation to the activity of a limited brain region within the homogeneous and the 3-shell spherical head models. This approximation should also be reasonable for realistic head models, because the deviations from sphericity should induce highly similar attenuations or amplifications of scalp potentials for intracranial sources which are close to each other. We may therefore accept the accuracy of the 3-shell head model and the regional dipole source concept at this stage and test the validity of this approximation with realistic data which usually exhibit more complex source configurations

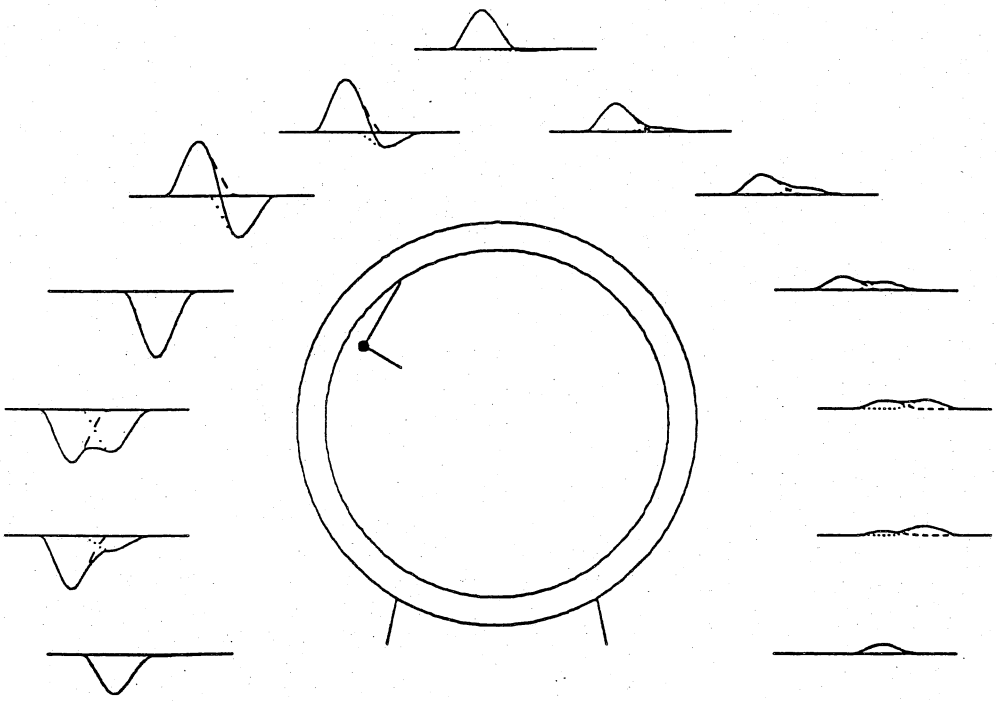

Fig. 7. Spatiotemporal overlap due to a radial and tangential pair of dipoles having the same location (= 2-dimensional regional source) and modeling one side of a cortical fissure (cf. fig. 1). The radial activity of the superficial cortical segments is assumed to be delayed and to start just after the tangential activity has peaked. Note the complexity of overlap in the waveforms simulated for the coronal eletrode montage. However, this presents the simplest example of overlap one can imagine. · · · = Radial activity; --- = tangential activity.

than those simulated so far. To understand how a hypothesis can be tested by modeling, next the mathematical approach to inverse solutions shall be outlined in detail.

A General Mathematical Approach to the Source Problem

Basic Equations

When we record a brain electric signal, we can only measure the potential difference between 2 electrodes placed at different scalp locations:

$$v_k(t) = u_k(t) - u_r(t) \tag{5}$$

with $u_k(t)$ being the potential at electrode k, $u_r(t)$ the potential at the reference electrode and $v_k(t)$ the bipolar voltage difference recorded in channel k. These signals are functions of time, usually sampled at a constant discrete time interval and may hence be written as vectors of dimension T:

$$v_k = |v_{k1}, v_{k2}, \ldots v_{kT}|; \qquad t = 1, 2, \ldots T.$$

The whole recorded data set can then be written as a matrix

$$v = |v_1, v_2, \ldots v_{NC}|' = |v_{ki}| \quad k = 1,2 \ldots NC$$

of dimension NC (= number of channels)·T, each row being the wave form recorded in one channel. Similarly, for the potential at each electrode (k = 1, 2, ... NE; NE=NC+1; NE = number of electrodes; the reference electrode must always be included for correctness!) a matrix U [NE·T] may be defined. The relation of the rows of U and the rows of V is given by equation 5. It is advantageous to transform the measured data set V into a matrix V′ (dimension NE·T) which is average referenced [Scherg and von Cramon, 1984], because then equal weight will be given to each electrode in the following computations by

$$v'_{kt} = u_{kt} - (1/NE) \sum_{i=1}^{NE} u_{it}. \tag{6}$$

Let NS be the number of equivalent sources for a given hypothesis. The compound activity of the i-th source shall be denoted by a wave form $s_i(t)$, or s_i in vector notation (i = 1, 2 ... NS). We shall scale this waveform also in voltage units and, because of the dipolar nature of the distant fields discussed above, we shall always use the term 'dipole source potential' to denote source activity without loss of generality. Note that for the full description of a 3-dimensional regional source also 3 dipole source potentials are required, i.e. 3 rows in the matrix S (NS·T).

The relation of the source activity, i.e. the dipole source potentials, and the potential at the scalp electrodes is illustrated in figure 8. A priori, one cannot assume that a pair of electrodes may be selected which would record activity only from a single source. Rather, each electrode e_k senses activity from each source s_i with a specific relative attenuation coefficient c_{ki}, depending on the geometrical configuration of the source and the location of the electrode relative to the source. For dipole sources, the contribution of source activity to the electrode potential depends on electrode location, source location, source orientation and on the conduction properties of the volume conductor.

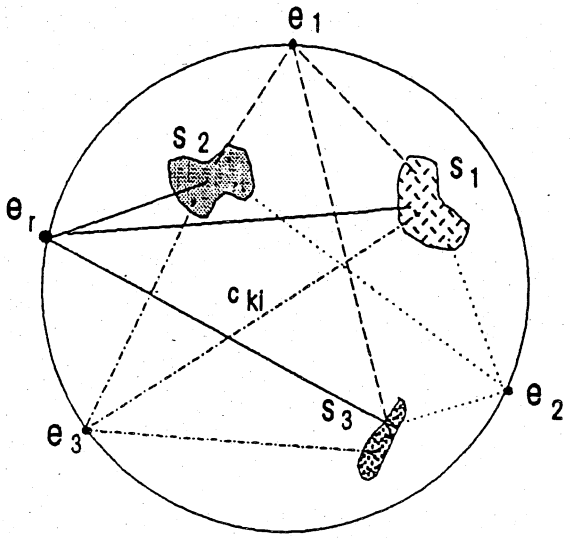

Fig. 8. Illustration of the direct linear approach to a deconvolution of the overlap due to multiple sources. Each source i (s_1–s_3) contributes to the potential at each electrode k (e_1–e_3) and at the reference e_r with a specific attenuation coefficient c_{ki}. This relation is linear, because increases and decreases of source strengths are proportionally reflected at each electrode, the proportion factor being c_{ki}. Spatial deconvolution is achieved by an inversion of the system of linear equations relating scalp and source activities.

There is only one physical law which must be inferred to formulate the source problem in mathematical terms, i.e. the superposition law holding for electric fields. This states that the potential at electrode k is the linear sum of the contributions from *all* sources:

$$u_k(t) = \sum_{i=1}^{NS} c_{ki} s_i(t), \tag{7}$$

or in matrix notation:

$$U = C\,S\,; \qquad C = \{c_{ki}\} \tag{8}$$

or

$$V' = C'\,S\,; \qquad C' = \{c'_{ki}\} = \{c_{ki} - c_{ri}\} \tag{9}$$

with C and C′ being matrices of geometrical weighting coefficients relating source, electrode and head geometry. When these coefficients are combined for each source in vector form [Scherg and von Cramon, 1986a], they are proportional to the electric lead field vectors [Hari and Ilmoniemi, 1986].

Real data consist of potential differences. Hence, it is important to subtract the contribution of the average reference (or of the common reference if V is used as input, which is given by the coefficient c_n. The coefficients c_{ki} are, apart from a common scale factor, identical to the head model function $f(\mathbf{r}_i, \mathbf{o}_i, \mathbf{e}_k)$ in equation 4.

Note that by this formulation, which includes time dependence, the source problem is defined as the task of separating the scalp potential matrix U into an electroanatomical, time-independent part (C matrix) and into a time-dependent dipole source potential matrix (S), which reflects the strength of each source varying over time and, thus, the compound physiological processes within the sources. The time independence of C implies that sources, akin to their anatomical substrate, do not move within the brain even though such a movement may phenomenologically appear at the scalp.

Therefore, in mathematical terms, the inverse problem resides in finding an adequate decomposition of the matrix U, respectively V′, into a source geometry matrix C and a source potential matrix S. This formulation is identical to the principal component analysis (PCA) approach [Glaser and Ruchkin, 1976], but the essential difference lies in the constraints imposed on the matrix C. While PCA maintains constraints related to mathematical concepts of orthogonality and communality in variance, the present approach enables constraints to be based on head geometry and volume conduction theory. A PCA approach incorporating dipole constraints has recently been presented by Maier et al. [1987].

Unique and Direct Solution for Dipole Source Potentials

In order to understand how and under which conditions the source problem can be solved, it is helpful to make a thought experiment. Assume for a moment that the source geometry is known or that a certain fixed source configuration is hypothesized. In this case all elements of the matrix C can be computed by locating a unit dipole at each source position and calculating the relative attenuation for each electrode-source configuration according to equation 4. Equations 7–9 then represent a system of NE linear equations. Of these only NC or less are linearly independent, i.e. as many as there are recording channels which are linearly independent. From linear algebra it is known that a unique solution to equations 7–9 can exist only if the number of sources (NS) is equal to the number of channels (NC). Given this condition, for any nonsingular matrix C a set of NS=NC values of source strengths s_1, s_2 ... s_{NS} can be computed for each time instance from the recorded voltage differences v_1, v_2, ... v_{NC} by inversion of equations 7–9:

$$S = C^{-1} U. \quad (10)$$

An example for this is illustrated in figure 9. Dipole source activity is simulated for a tangential and radial source in both auditory cortices. The scalp potentials show a complex overlap due to the activity of the 4 sources. But, a 4-channel recording is sufficient for an inverse computation of the 4 dipole source potentials, if the location of the 2 regional sources is known.

If NS is less than NC then equations 7–9 present an overdetermined system of linear equations and C^{-1} in equation 10 is replaced by the pseudoinverse matrix of C (C^p) computed by linear optimization, e.g. using the Householder algorithm. In this case, the recomputed model waveforms at the scalp

$$U' = C S = C C^p U \neq U \quad (11)$$

are not equal to the measured waveforms, but the difference between the 2 matrices $U' - U$ is implicitly minimized, i.e. a best fit of the model to the measured data is achieved for the given hypothesis. Also in this case, the larger number (NC) of scalp waveforms is reduced to a smaller set of unique dipole source potentials (NS). Examples for this are illustrated in figures 10 and 11. Note that the derivation of the dipole source potential matrix S is independent of the reference electrode, because the optimization algorithm computes the minimal norm of the matrix C. A principally similar mathematical approach, 'the software lens', has been presented by Freeman [1980] for the spatial deconvolution of the surface EEG from the olfactory bulb and is described in detail by Nunez [1981].

The Iterative Direct Approach: Finding Source Locations

So far, it has been assumed that C is known on the basis of some anatomical hypotheses, but now the steps for the computation of the source parameters underlying C will also be outlined. If there are more channels to be determined than sources, the additional information in the scalp waveforms can be used to extract information about the source configuration itself, i.e. to determine some relevant parameters which underly the matrix C, i.e. source locations r_i and orientations o_i according to equation 4. Thus, for each dipole source, 5 unknown parameters are to be determined, in addition to the dipole source potentials $s_i(t)$. Because the head model function (eq. 4) is nonlinear, a solution has to be found by an iterative procedure. This will be shortly illustrated because it is essential for the understanding of the modeling approach.

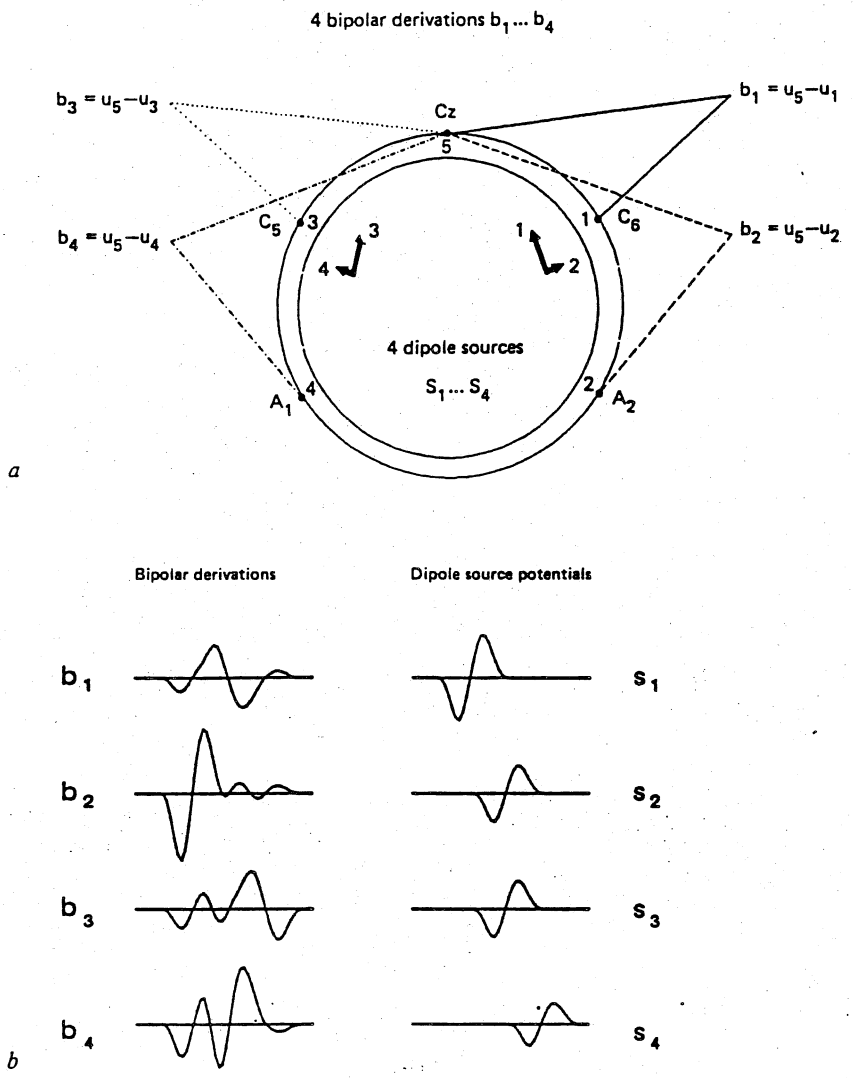

Fig. 9. Simulated example of the extraction of bilateral temporal lobe dipole source potentials from a 4-channel measurement. The 4 bipolar scalp derivations can be linearly transformed into 4 source potential waveforms associated with bilateral tangential and radial dipole sources in the auditory cortex (top: back view of the head model coronal section). Note the complexity of waveforms in the scalp derivations (b_1–b_4) resulting from different overlap of the assumed simple biphasic source activities (bottom). In this example, the transformation is unique for any set of 4 fixed dipoles. But, if looked at as an inverse problem, the location of the dipoles could not be extracted unless more channels were recorded.

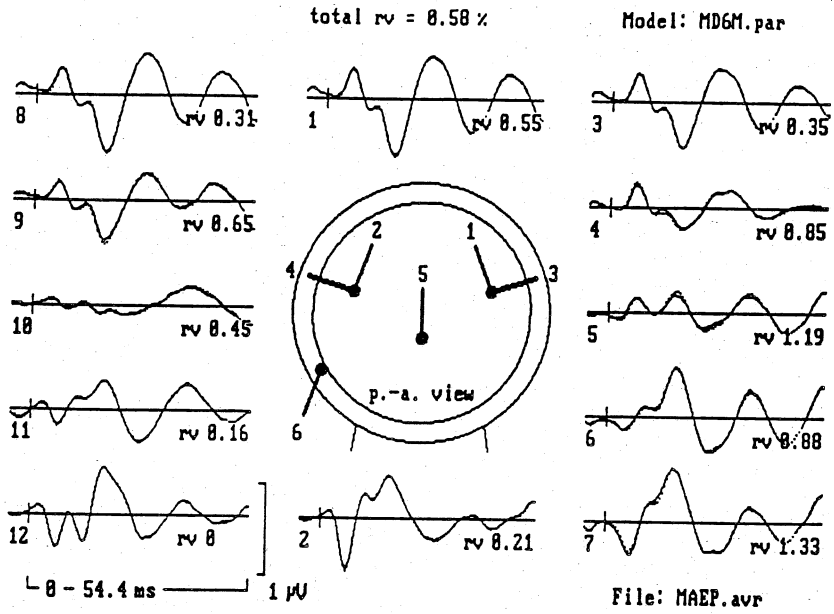

Fig. 10. Coronal MAEP scalp distribution measured in a normal subject (—). Right ear stimulation with 70 dB HL clicks, 10,000 sweeps averaged. Both the early slow ABR and the middle-latency vertex N_a–P_a (N19–P30) transient show a widespread distribution with apparent polarity reversals between upper and lower electrode sites. Different waveforms are revealed at lateral electrodes 5 and 10, because the data were average referenced; this leading to virtual zero at the height of the superior temporal gyrus for this coronal montage. The head model inset shows the final best-fit dipole configuration using model D. Due to the negligible residual variance (RV) of 0.58%, the model waveforms (···) coincide almost everywhere with the measured waveforms. p.-a. = Posterior-anterior.

First, one chooses a starting hypothesis with some reasonable starting locations and orientations for each source. The assumed number of sources must be less than the number of recording channels. Next, a dipole source potential solution is found using equation 10, a model waveform matrix U′ is computed by equation 11 and the unexplained residual variance (RV) is calculated by comparing model and measured data matrices [Scherg, 1984]. Then, iteratively one or more source parameters are changed, i.e. dipole sources are shifted in location or orientation, and the same computations are repeated. Changes in source parameters decreasing RV are accepted until RV, i.e. the difference between model and measured data, is minimized. The resulting

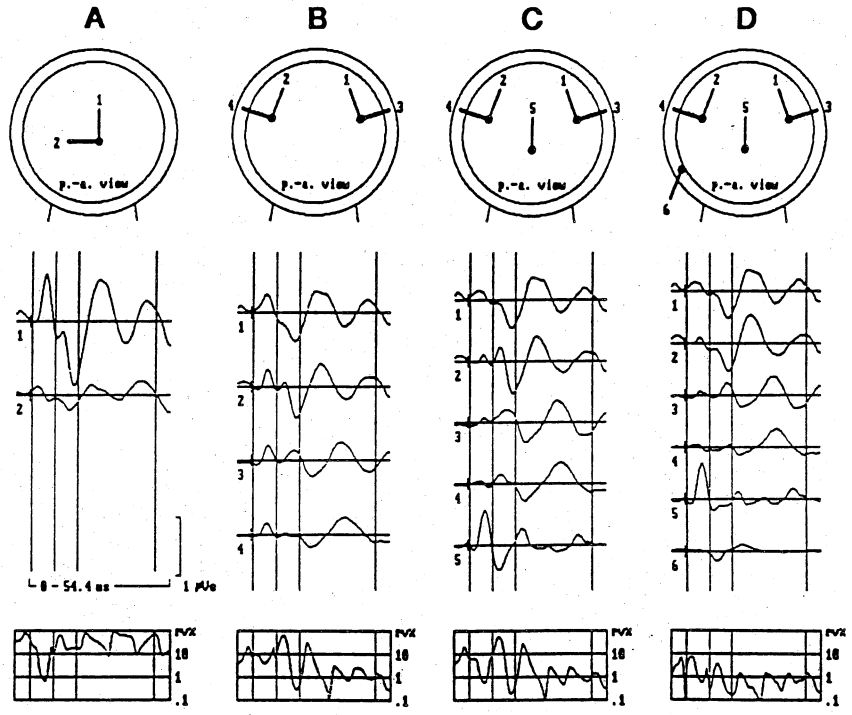

Fig. 11. Dipole source potentials and residual variance (RV) as evaluated from the MAEP data of figure 10 for 4 different hypotheses (A-D). Vertical bars mark the 3 latency intervals 1–10 ms, 10–19 ms and 19–49 ms, for which RV was evaluated. The central source is necessary to explain the early slow ABR activity (A, C, D) as shown by minimal RV in the early interval. In the middle-latency range (19–49 ms) bilateral temporal lobe sources are required for minimal RV (B, C, D). Note the similar dipole source potentials in both hemispheres and the delayed activity of the radial as compared to the tangential temporal lobe sources. In model C, dipole source potential waveforms exhibit an unexplained interference in the 10- to 26-ms latency range. Addition of a scalp source (dipole 6, model D) removes this interference and extracts the waveform of the underlying postauricular muscle reflex with peaks at 13 and 24 ms. p.-a. = Posterior-anterior.

source configuration presents the best model fit for the given number of sources in the whole time epoch analyzed. Such an iterative procedure is called a nonlinear least-squares fit and may be implemented using different algorithms [Schneider, 1972; Scherg, 1984; Fender, 1987]. By the implicit use of a matrix inversion (eq. 10), the number of parameters to be adjusted by the time-consuming iteration algorithm is greatly reduced. Only the spatial parameters

are to be adjusted, while the temporal parameters, i.e. the dipole source potentials, are determined by the direct linear approach (eq. 10).

However, if also the matrix S is parametrized, e.g. by the latencies and amplitudes of peaks in dipole source potentials, the inverse problem can be treated as a complete nonlinear problem and the temporal parameters are then found by iteration, too. Such a spatiotemporal dipole model [Scherg, 1984; Scherg and von Cramon, 1985a, b] allows for an even greater data reduction by temporal restrictions on the dipole source potential waveforms. Both the direct linear approach, illustrated here, and the spatiotemporal dipole model have yielded comparable results for cortical AEP activity [Scherg and von Cramon, 1986a].

Conventional instantaneous dipole localization methods use similar iterative procedures to determine the 6 coordinates (x, y, z, m_x, m_y, m_z) of a single dipole or the 12 coordinates of 2 dipoles solving the nonlinear system of equations (eq. 3) for a given set of instantaneous voltages $[v_1, v_2, \ldots v_{NC}]$ recorded in NC channels [Schneider, 1972; Kavanagh et al., 1978; Gulrajani et al., 1984; Fender, 1987]. Note that the head model function (eq. 3) must be determined for all electrodes, including the reference electrode (preferably average reference), and that the potential differences according to equation 5 must be fitted by the model function [Schneider, 1972]. The set of equations (eq. 3) for a fixed time instance, as used in conventional dipole localization methods, presents just a special case of the more general spatiotemporal formulation (eq. 7–9).

Aspects of Data Reduction

The information contained in a whole series of spatiotemporal maps or scalp waveforms, respectively, is condensed into a small number of equivalent source parameters and dipole source potentials using the presented approach. If only a single instantaneous map is analyzed, then for a single dipole source 6 parameters have to be determined (3 location coordinates, 2 orientation angles and dipole strength) and at least the same number of recording channels is required for a unique solution. For each further source, 6 additional linear independent channels would be required. But to obtain a stable solution at least twice as many channels as unknown parameters would be reasonable [Fender, 1987]. Thus, under realistic conditions, from a single map hardly more than 2 dipoles can be determined unambiguously.

When a longer time epoch is analyzed at once, the situation becomes different. There are instances when one source is strong and the others are weak and vice versa. With the concept of the stationary regional dipole

source, the information on the source configuration is extracted not from a single map but over the whole epoch. Hence, more dipole sources can be located, if these sources change in strength asynchronously, i.e. if their dipole source potentials are not correlated 100%. Again, as for the single dipole, a minimum of 6 channels is required to obtain 3 independent location parameters in addition to dipole strength and orientation angles. But from an 8-channel recording, for example, not only 1 but 4 or 5 sources could be determined and their overlap disentangled over time.

What would the data reduction be in that case? Assume, we have 50 digitization points in each channel, only 10 of which may contain relevant information (peak amplitudes, latencies, zero crossings), i.e. d.f. = 8*10 = 80. If we select 10 different times and compute a single equivalent dipole at each time (not separating the overlap!), the 80 parameters are condensed into 60, not considering that times other than the preselected may contain further information. Reducing the 8 channels to 4 dipole source potentials results in 40 parameters plus 5 parameters per source, i.e. 5*4=20. Still, there is the same amount of data reduction, but we have located and separated 4 sources over time and not only a single dipole which may be a poor explanation of the data at many times. With 5 sources (d.f. = 75) the parameter space would still not be exhausted.

In addition, spatial parameters can be further reduced by using the concept of regional sources, i.e. 3 dipole components share the same location parameters. Also, hemispheric symmetry in location can be used as a constraint to further reduce the number of spatial parameters. For the auditory cortex, which is located fairly symmetric in both temporal lobes, this presents a reasonable restriction leading to very stable results. Taking the above example, data reduction for the 2-dimensional auditory-evoked-potential model would be to 40 time + 2 spatial parameters only, irrespective of whether 8 or 12 channels have been recorded in the coronal plane (as e.g. in fig. 11, B).

A Realistic Example: Middle-Latency Auditory-Evoked Potentials

The middle-latency auditory-evoked potentials (MAEP) present a challenging example to test the power of dipole source potential analysis because in this time range overlap of multiple myogenic and neurogenic activities occurs [Streletz et al., 1977; Scherg and Volk, 1983]. Sources in centrally located structures, e.g. in the brainstem and thalamus, in lateral structures,

i.e. in the auditory cortex, and in superficial muscles, e.g. in the postauricular muscle can be anticipated. Accordingly, we may formulate hypotheses including central, bilateral and superficial dipoles and test these with measured MAEP scalp distributions.

In figure 10 the coronal scalp distribution of MAEPs elicited by 70 dB HL right ear click stimuli in a 38-year-old normal male subject is shown. A detailed description of recording methods has been presented elsewhere [Scherg and von Cramon, 1986a] along with 3 different spatiotemporal analyses of the same data set [Scherg and von Cramon, 1986a, fig. 2]. In these previous analyses, only the dipole source potentials due to the temporal lobe sources have been depicted. Here, we will illustrate in more detail, how the final solution, consisting of 6 equivalent dipoles (fig. 10), can be gained using the direct approach, which has been presented above and which is identical to approach (b) in Scherg and von Cramon [1986a].

If we hypothesize only a single regional source to account for the 2-dimensional potential distribution of the MAEP in the coronal plane, central locations close to the middline are found for this source throughout the time course of the MAEP. The location is slightly below the center of the spherical head model, when the residual variance is minimized in an early interval of 1–10 ms after stimulation (fig. 11, A), and about half way up the head model for a middle-latency interval of 19–49 ms. Inspection of the residual variance plotted over time shows a best fit in the early time range at the peak of the slow auditory brainstem response (slow ABR), which also presents the first major positive deflection in the vertical dipole source potential (6.4 ms, fig. 11 A, dipole 1). The horizontal dipole source potential of the central regional source exhibits an even earlier deflection (3.4 ms, dipole 2) representing the slow ABR associated with activity of 2nd-order afferents crossing the lower brainstem [Scherg and von Cramon, 1985b]. But for this single regional source hypothesis, the residual variance plot shows a poor fit both in the middle latency (19–49) and in the intermediate interval of 10–19 ms (table 1). In this interval, a myogenic reflex can be seen at electrode 12 (fig. 10) and in the vertical dipole source potential, which peaks at 13 ms between the slow auditory brainstem response and N19 (fig. 11, A).

The converse situation occurs if we hypothesize bilaterally symmetric temporal lobe sources. The activity of each temporal region is approximated by a tangential and a radial dipole in our 2-dimensional set-up. With these restrictions, only the 2 spatial parameters – eccentricity and the angle theta of the location vector with the vertical z-axis – must be determined in addition to the 4 dipole source potentials. The best-fit location, minimizing the

Table 1. Residual variances (%) for 4 different hypotheses modeling the MAEP of a normal subject as depicted in figure 11

Dipole configuration			Model	Latency range		
temporal	central	myogenic		1–10 ms	10–19 ms	19–49 ms
–	2/1 RS	–	A	*2.2*	18.8	15.7
4/2 RS	–	–	B	5.3	5.2	*2.3*
4/2 RS	1	–	C	*1.3*	4.4	2.1
4/2 RS	1	1	D	1.0	*0.6*	*0.5*

n/n RS = Number of dipoles/number of regional sources.

residual variance in the 19- to 49-ms interval, and the related 4 dipole source potentials are depicted in column B of figure 11. The residual variance plot exhibits a poor fit in the early, slow ABR range, but an excellent fit for N19 and at all latencies above 19 ms. However, if we add a vertical midline dipole at the height of the brainstem to our model, the residual variance in the 1- to 10-ms interval becomes very small again and – this being the important finding – the overlapping activities of the central source (dipole 5: slow ABR) and of the temporal lobe tangential (dipoles 1–2: N19t–P30t transient) and radial (dipoles 3–4: N27r–P39r transient) sources are clearly separated in the dipole source potential waveforms (fig. 11, C).

If only the 4 temporal lobe dipoles are used, the early activity is not correctly accounted for by an equivalent source and, hence, is projected with some attenuation onto the 4 dipole source potentials (fig. 11, B, C), whereas the later activity is not much affected by the presence or absence of an additional central source. Note that the horizontal dipole of the central regional source could not be added to the model because it would have strongly interacted with the almost colinear dipoles 3 and 4. Thus, noise in the data and inaccuracies of the head model restrict the spatial resolution of horizontal activity in the 12-electrode array used in this example.

By using the 5- instead of the 4-dipole model, the unexplained residual variance around 13 and 22 ms was not improved. This indicated overlap from another source and suggested to fit a further dipole to minimize the residual variance in the intermediate 10- to 19-ms interval. The resulting 6 dipole model showed an additional superficial dipole (dipole 6, fig. 11, D) underlying the left earlobe electrode. Its dipole source potential reflects

activity of the postauricular muscle peaking at 13 and 22 ms. Although the magnitude of this activity is small, its superficial location leads to considerable overlap in scalp potential waveforms (fig. 10) and to interactions between the other dipole source potentials if not accounted for (cf. the negative peak at 13 ms in DSP 5, and the positive peak in DSP 2, fig. 11, C). By the way, exclusion of electrode 12 (fig. 10) from the analysis similarly removed this interaction and yielded almost identical waveforms for the first 5 dipoles.

Residual variances for the 4 different hypotheses A–D, as depicted in figure 11, are given in table 1, showing clear improvements of the model in the time intervals for which addition of further dipoles was necessary (italicized values). Note that using the last model (D) with 6 dipoles the 12-scalp potential waveforms (fig. 10) have been reduced and transformed into 6 dipole source potentials (fig. 11) with an overall residual variance of only 0.58%. Thus, 99.4% of the scalp potential variance in space and time has been explained by proposed compound activities in distinct brain areas. In addition, the waveforms of the resultant dipole source potentials exhibit a clear separation between the early slow ABR, intermediate myogenic and the middle-latency auditory-cortical activities, which commence with the N19t–P30t transient.

Conclusions

As illustrated by the last example, the main advantage of dipole source potential analysis appears to be its principal capability of disentangling the overlap inherent in scalp potential waveforms and maps. But what about the reliability of the solution? First of all, the waveforms of the dipole source potentials are very robust against inaccuracies in source location and head model, as long as the interaction between dipoles remains small. This reflects the observation of Stok et al. [1987] that more stable estimates of the dipole moment can be obtained from electric recordings, whereas estimates of source location are more accurate when based on magnetic field recordings. The robustness of dipole source potential waveforms can be seen easily when changes in the order of 10% in eccentricity or angles of the source location vector are tested. This leads to only small increases in residual variance (on the order of 0.5%) as compared to much larger reductions obtained by adding appropriate additional dipoles. Note that the type of evoked activity, noise in

the data, the number of recording channels and inaccuracies in the head model limit the number of dipoles which can be reliably extracted. In our example, the overall residual variance of 0.58% and the low residual variances in all 3 analysis intervals (table 1) prohibited an increase in the number of simultaneous dipoles beyond 6.

In any case, the stepwise testing of different hypotheses, as shown, will give keys toward realistic models of any type of evoked potentials. These can then be further and independently tested in patients with circumscribed lesions. Such an ultimate check for the validity of the presented model as applied to middle- and late-latency auditory-evoked potentials is presented in more detail in Scherg and von Cramon [1986a, b, 1990, this volume]. Finally, I hope that this chapter has illustrated the value of simulations and modeling in an attempt to understand the spatiotemporal complexity of evoked electrical scalp activity.

Acknowledgments

I wish to thank Jos Eggermont for helpful comments on the manuscript and Jutta Dinkel for secretarial help.

References

Ary, J.P.; Klein, S.A.; Fender, D.H.: Location of sources of evoked scalp potentials: corrections for skull and scalp thicknesses. IEEE Trans. biomed. Engng *28:* 447–452 (1981).

Brody, D.A.; Terry, F.H.; Ideker, R.E.: Eccentric dipole in a spherical medium: generalized expression for surface potentials. IEEE Trans. biomed. Engng *20:* 141–143 (1973).

Cuffin, B.N.; Cohen, D.: Comparison of the magnetoencephalogram and electroencephalogram. Electroenceph. clin. Neurophysiol. *47:* 132–146 (1979).

Lesmedt, J.E.; Nguyen, T.H.; Bourguet, M.: Bit-mapped color imaging of human evoked potentials with reference to the N20, P22, P27, and N30 somatosensory responses. Electroenceph. clin. Neurophysiol. *68:* 1–19 (1978).

Duffy, F.H.; Burchfiel, J.L.; Lombroso, C.T.: Brain electrical activity mapping (BEAM): a method for extending the clinical utility of EEG and evoked potential data. Ann. Neurol. *5:* 309–321 (1979).

Fender, D.H.: Source localization of brain electrical activity; in Gevins, Remond, Methods of analysis of brain electrical and magnetic signals; EEG Handbook, revised series, vol. 1, pp. 355–403 (Elsevier, Amsterdam 1987).

Freeman, W.J.: Use of spatial deconvolution to compensate for distortion of EEG by volume conduction. IEEE Trans. biomed. Engng *27:* 421–429 (1980).

Glaser, E.M.; Ruchkin, D.S.: Principles of neurobiological signals analysis (Academic Press, New York 1976).

Grandori, F.: Dipole localization methods (DLM) and auditory-evoked brainstem potentials. Revue Lar. Otol. Rhinol. *105:* 171–178 (1984).

Grandori, F.: Field analysis of auditory evoked brainstem potentials. Hearing Res. *21:* 51–58 (1986).

Gulrajani, R.M.; Roberge, F.A.; Savard, P.: Moving dipole inverse ECG and EEG solutions. IEEE Trans. biomed. Engng. *31:* 903–910 (1984).

Hämäläinen, M.S.; Sarvas, J.: Realistic conductivity geometry model of the human head for interpretation of neuromagnetic data; Report TKK-F-A614, Helsinki University of Technology, pp. 1–19 (1987).

Hari, R.: The neuromagnetic method in the study of the human auditory cortex; in Grandori, Hoke, Romani, Auditory evoked magnetic fields and electric potentials. Adv. Audiol., vol. 6, pp. 222–282 (Karger, Basel 1990).

Hari, R.; Ilmoniemi, R.J.: Cerebral magnetic fields. CRC critic. Rev. biomed. Engng *14:* 93–126 (1986).

Kavanagh, R.N.; Darcey, T.M.; Lehmann, D.; Fender, D.H.: Evaluation of methods for three-dimensional localization of electrical sources in the human brain. IEEE Trans. biomed. Engng *25:* 421–429 (1978).

Lehmann, D.; Skrandies, W.: Reference-free identification of components of checkerboard-evoked multichannel potential fields. Electroenceph. clin. Neurophysiol. *48:* 609–621 (1980).

Maier, J.; Dagnelie, H.; Spekreijse, H.; van Dijk, B.W.: Principal components analysis for source localization of VEPs in man. Vision Res. *27:* 165–177 (1987).

Meijs, J.W.H.; Bosch, F.G.C.; Peters, M.J.; Lopes da Silva, F.H.: On the magnetic field distribution generated by a dipolar current source situated in a realistically shaped compartment model of the head. Electroenceph. clin. Neurophysiol. *66:* 286–298 (1987).

Meijs, J.W.H.; Peters, J.M.; van Oosterom, A.: Computation of MEGs and EEGs using a realistically shaped multi-compartment model of the head. Med. biol. Engng Comput. *23:* suppl. pp. 36–37 (1985).

Mitzdorff, U.: Current source-density method and application in cat cerebral cortex: investigation of evoked potentials and EEG phenomena. Physiol. Rev. *65:* 37–91 (1985).

Nunez, P.L.: Electrical fields of the brain (Oxford University Press, New York 1981).

Plonsey, R.; Heppner, D.B.: Considerations of quasi-stationarity in electrophysiological systems. Bull. math. Biophys. *29:* 657–664 (1967).

Rall, W.: Time constants and electrotonic length of membrane cylinders and neurons. Biophys. J. *9:* 1483–1508 (1969).

Rush, S.; Driscoll, D.A.: Current distribution in the brain from surface electrodes. Anaesthesia Analgesia current Res. *47:* 717–723 (1968).

Scherg, M.: Spatio-temporal modelling of early auditory-evoked potentials. Revue Lar. Otol. Rhinol. *105:* 163–170 (1984).

Scherg, M.; Cramon, D. von: Topographical analysis of auditory of auditory evoked potentials: derivation of components; in Nodar, Barber, Evoked potentials. Part II, pp. 73–81 (Butterworths, Woburn 1984).

Scherg, M.; Cramon, D. von: Two bilateral sources of the late AEP as identified by a spatio-temporal dipole model. Electroenceph. clin. Neurophysiol. *62:* 32–44 (1985a).

Scherg, M; Cramon, D. von: A new interpretation of the generators of BAEP waves I–V: results of a spatio-temporal dipole model. Electroenceph. clin. Neurophysiol. *62:* 290–299 (1985b).

Scherg, M.; Cramon, D. von: Evoked dipole source potentials of the human auditory cortex. Electroenceph. clin. Neurophysiol. *65:* 344–360 (1986a).

Scherg, M.; Cramon, D. von: Psychoacoustic and electrophysiologic correlates of central hearing disorders in man. Eur. Archs Psychiat. Neurol. Sci. *236:* 56–60 (1986b).

Scherg, M.; Cramon, D. von: Dipole source potentials of the auditory cortex in normal subjects and in patients with temporal lobe lesions; in Grandori, Hoke, Romani, Auditory evoked magnetic fields and electric potentials. Adv. Audiol., vol. 6, pp. 165–193 (Karger. Basel 1990).

Scherg, M.; Volk, S.A.: Frequency specificity of simultaneously recorded early and middle latency auditory evoked potentials. Electroenceph. clin. Neurophysiol. *56:* 443–452 (1983).

Schneider, M.R. A multistage process for computing virtual dipolar sources of EEG discharges from surface information. IEEE Trans. biomed. Engng *19:* 1–2 (1972).

Sidman, R.D.; Giambalvo, V.; Allison, T.; Bergey, P.: A method for localization of sources of human cerebral potentials evoked by sensory stimuli. Sensory Processes. *2:* 116–129 (1978).

Stok, C.J.: Meijs, J.W.H.: Peters, M.J.: Inverse solutions based on MEG and EEG applied to volume conductor analysis. Phys. Med. Biol. *32:* 99–103 (1987).

Streletz, L.J.; Katz, L.; Hohenberger, M.; Cracco, R.Q.: Scalp recorded auditory evoked potentials and sonomotor responses: an evaluation of components and recording techniques. Electroenceph. clin. Neurophysiol. *43:* 192–206 (1977).

Vaughan, H.G., Jr.: The analysis of scalp-recorded brain potentials; in Thompson, Patterson, Bioelectric recording techniques, Part B, pp. 158–207 (Academic Press, New York 1974).

Wilson, F.N.; Bayley, R.H.: The electric field of an eccentric dipole in a homogeneous spherical conducting medium. Circulation *1:* 84–92 (1950).

Wood, C.C.: Application of dipole localization methods to source identification of human evoked potentials. Ann. N.Y. Acad. Sci. *388:* 139–155 (1982).

Michael Scherg, PhD. Max Planck Institute for Psychiatry, Department of Neuropsychology, Psychoacoustics and Evoked Potentials Laboratory, Kraepelinstrasse 10, D–8000 Munich 40 (FRG)